Luminescent Antimony Halides Hot Paper

How to cite: *Angew. Chem. Int. Ed.* **2023**, *62*, e202216720
International Edition: doi.org/10.1002/anie.202216720
German Edition: doi.org/10.1002/ange.202216720

Achieving Near-unity Photoluminescence Quantum Yields in Organic-Inorganic Hybrid Antimony (III) Chlorides with the [$SbCl_5$] Geometry

*Chen Sun, Zeyu Deng, Zhiyuan Li, Zhongwei Chen, Xuanyu Zhang, Jian Chen, Haipeng Lu, Pieremanuele Canepa, Rui Chen, and Lingling Mao**

Abstract: Hybrid organic–inorganic antimony halides have attracted increasing attention due to the non-toxicity, stability, and high photoluminescence quantum yield (PLQY). To shed light on the structural factors that contribute to the high PLQY, five pairs of antimony halides with general formula A_2SbCl_5 and $A_2Sb_2Cl_8$ are synthesized via two distinct methods and characterized. The A_2SbCl_5 type adopts square pyramidal [$SbCl_5$] geometry with near-unity PLQY, while the $A_2Sb_2Cl_8$ adopts seesaw dimmer [Sb_2Cl_8] geometry with PLQY $\approx$ 0 %. Through combined data analysis with the literature, we have found that A_2SbCl_5 series with square pyramidal geometry generally has much longer Sb···Sb distances, leading to more expressed lone pairs of Sb^{III}. Additional factors including Sb–Cl distance and stability of antimony chlorides may also affect PLQY. Our targeted synthesis and correlated insights provide efficient tools to precisely form highly emissive materials for optoelectronic applications.

Introduction

Hybrid organic–inorganic metal halides show great potentials for a variety of optoelectronic applications such as solar cells[1,2] and light-emitting diodes.[3–5] They are highly flexible with organic counterparts,[6] inorganic metals,[7] and halide components.[8] For example, hybrid lead halide perovskite materials have demonstrated highly diverse structural, optical, and electronic properties with the templating effects of organic cations and halide variations.[9–11] More recently, hybrid antimony halides have attracted increasing attention as alternatives because they are non-toxic comparing to lead, yet maintain good stability compare to other main group metals such as Ge^{2+} and Sn^{2+}.[9,12–14] Furthermore, Sb^{3+} has dynamic lone pairs[15,16] and has been widely used as an efficient dopant in many non-emissive systems to activate photoluminescence (PL) emission.[17–19]

In particular, zero-dimensional (0D) hybrid antimony halides have been reported with near-unity PLQY.[8,13,16,20–23] For example, $(MePPh_3)_2SbCl_5$,[24] $[TEA]_2SbCl_5$ (TEA^+ = tetraethylammonium),[25,26] $(TEBA)_2SbCl_5$ ($TEBA^+$ = tetraethylbenzylammonium),[25,26] $(PPN)_2SbCl_5$ (PPN^+ = bis(triphenylphosphoranylidene)-ammonium),[27] and $(DTA)_2SbCl_5$·DTAC (DTAC = dodecyl trimethyl ammonium chloride) all have PLQY > 90 %.[28] Unlike the antimony chlorides, other halides such as antimony bromides generally produce lower PLQY.[29,30] Lower dimensional perovskites, especially 0D metal halides usually have self-trapped exciton (STE) that promotes efficient broadband emission.[31–34] Therefore, selecting bulky organic cations to isolate the metal halide and intentionally aim for 0D structures to have better PL performances is of particular interests.[13,33]

Previously, we have found a correlation between Mn···Mn distances and PLQY in 0D hybrid Mn^{II} bromides, where longer Mn···Mn distances lead to higher PLQY.[35] It is possible to extend this principle into the 0D antimony chlorides to find a clear structure–property relationship. Moreover, we want to explore this correlation with no other factors such as types of organic cations and presents of hydrogen bonding interactions. The optimal condition to investigate this relationship is to compare two different structures that possess exactly the same organic cation and metal halide in two different coordination environments. However, alternating structures with the same composition is difficult to achieve. In addition, to deliberately control the formation of specific coordination mode is not as common. There are few studies that are able to fine tune the properties of the desired product via kinetic-

[*] Dr. C. Sun, Z. Li, Dr. J. Chen, Prof. Dr. L. Mao
Department of Chemistry, Southern University of Science and Technology
Shenzhen, Guangdong, 518055 (China)
E-mail: maoll@sustech.edu.cn
Dr. Z. Deng, Prof. Dr. P. Canepa
Department of Chemical and Biomolecular Engineering, National University of Singapore
EA, Singapore 117575 (Singapore)
Z. Chen, Prof. Dr. H. Lu
Department of Chemistry, The Hong Kong University of Science and Technology
Kowloon, Hong Kong (Hong Kong)
X. Zhang, Prof. Dr. R. Chen
Department of Electrical and Electronic Engineering, Southern University of Science and Technology
Shenzhen, Guangdong, 518055 (China)

thermodynamic,[36,37] supramolecular,[13,30] or synthetic[29] approaches. For instance, Liu et al. demonstrated using different solvents can obtain $(Bmpip)_3Sb_2Br_9$ and $(Bmpip)_2SbBr_5$ that has PLQY of <1 % and 11.5 %, respectively.[29]

In order to control the formation of targeted structures and properties, we have utilized solvent engineering strategies and conducted parallel comparisons between two distinct phases. Here, we systematically synthesize and characterize ten (five pairs with each pair sharing the same organic cation *A*) 0D hybrid antimony chlorides to do a full analysis on their structural, optical, and electronic properties. Specifically, they are divided into two types due to the different coordination environment of Sb^{3+}, A_2SbCl_5 and $A_2Sb_2Cl_8$ (as shown in Scheme 1), where *A* represents five different organic cations: trimethylbenzyl ammonium = $(Me_3BzN)^+$; triethylbenzyl ammonium = $(Et_3BzN)^+$; tripropylbenzyl ammonium = $(Pr_3BzN)^+$; tetraethyl ammonium = $(Et_4N)^+$; tetrapropyl ammonium = $(Pr_4N)^+$).

The systematic patterns we have found in these antimony chlorides demonstrate the strong structural effect in their optical properties, especially showing significant contrast in PLQY. The square pyramidal $[SbCl_5]$ structural type synthesized by diffusion method in N,N-Dimethylformamide (DMF) with general formula A_2SbCl_5 shows high PLQY, large separation by the organic cation *A*, and lone pair highly expressed (scheme 1). On the other hand, the seesaw dimer type ($A_2Sb_2Cl_8$) can be obtained via solution method in HCl, resulting in significantly smaller Sb···Sb separation, lone pair repulsion and non-emissive PL properties. Combining our results and previous literature, we have found a correlation between the coordination environment of Sb, the Sb···Sb distance, and the PLQY. We further compare the optical and electronic properties of these two groups and reveal their signature differences. The solvent engineering strategy that successfully leads to two distinct structural types has tremendous potential for generalization in other systems. The precise control of structures and in-depth structural analysis enable us to provide powerful insights towards highly emissive hybrid materials for optoelectronics.

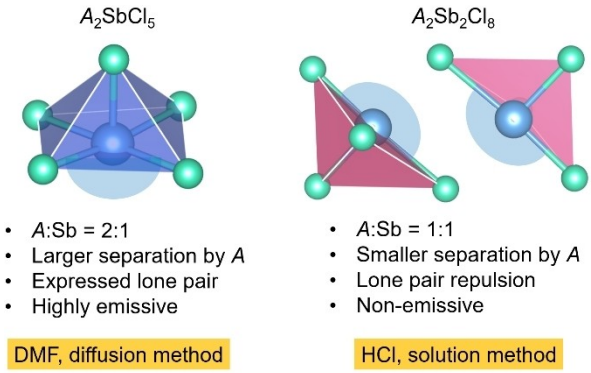

Scheme 1. Illustration of perspective for comparison of the A_2SbCl_5 and $A_2Sb_2Cl_8$ series.

Results and Discussion

Two synthetic approaches were performed to obtain the A_2SbCl_5 and $A_2Sb_2Cl_8$ coordination environment using the same organic cation. Hence, each organic templating cation generates two polymorphs with different stoichiometry in two solvent environments. Though some of the antimony chlorides have been previously reported (references have been given in Table 1), the structures were recollected and the crystallographic information can be found in the Supporting Information. Note that the formula for the $A_2Sb_2Cl_8$ can be simplified as $ASbCl_4$. However, due to the structural nature of the seesaw dimers, which always appear as a pair, we have decided to refer to this particular type as $A_2Sb_2Cl_8$. For A_2SbCl_5 containing 5-coordinated antimony chlorides (Figure 1a), the products were generated in DMF and crystallized using diethyl ether (Et_2O) as an antisolvent. For $A_2Sb_2Cl_8$ containing 4-cooridnated antimony chlorides (Figure 1b), the products were synthesized via heating all reagents in concentrated hydrochloric acid (HCl) followed by cooling to room temperature. A control experiment was done where over 10 equivalents of organic chloride salt were added to the reaction mixture during synthesis of the

Table 1: Comparison between the Sb–Cl bond lengths of the A_2SbCl_5 and $A_2Sb_2Cl_8$ series.

Organic Cation		$(Me_3BzN)^+$	$(Et_3BzN)^+$	$(Pr_3BzN)^+$	$(Et_4N)^+$	$(Pr_4N)^+$
Sb–Cl axial (Å)	$[SbCl_5]$	2.41	2.37	2.37	2.38	2.36
	$[Sb_2Cl_8]$	2.37	2.37	2.35	2.40	2.36
Longest Sb···Cl equatorial (Å)	$[SbCl_5]$	2.69	2.67	2.63	2.61	2.65
	$[Sb_2Cl_8]$	2.94	2.90	3.18	3.27	3.13
Shortest Sb···Cl equatorial (Å)	$[SbCl_5]$	2.59	2.56	2.55	2.59	2.57
	$[Sb_2Cl_8]$	2.44	2.43	2.42	2.40	2.34
Shortest Sb···Sb distances (Å)	$[SbCl_5]$	9.00	8.80	10.03	9.49	9.69
	$[Sb_2Cl_8]$	4.21	4.23	4.52	4.31	4.18

*Structures of $(Me_3BzN)_2SbCl_5$,[38] $(Et_3BzN)_2SbCl_5$,[25,26] $(Pr_3BzN)_2SbCl_5$,[39] $(Me_3BzN)_2Sb_2Cl_8$,[40] and $(Et_3BzN)_2Sb_2Cl_8$[40] are recollected experimentally and confirmed with literature reports. Structural information of $(Et_4N)_2SbCl_5$,[25,26] $(Et_4N)_2Sb_2Cl_8$,[41,42] $(Pr_4N)_2SbCl_5$,[43] and $(Et_4N)_2Sb_2Cl_8$[42] are directly from reported structures.

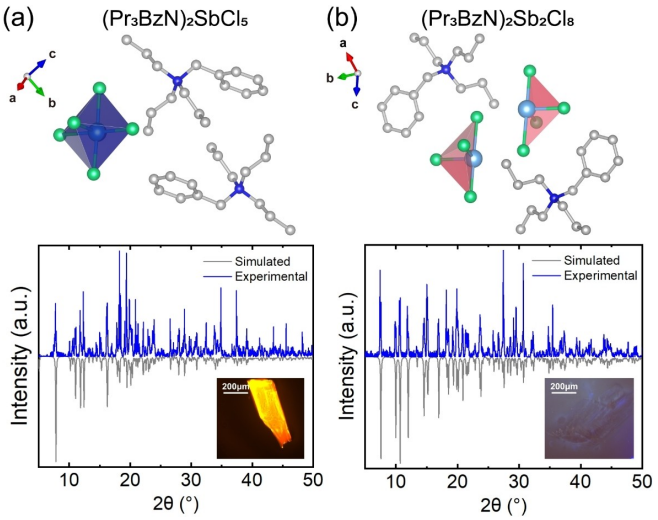

Figure 1. Crystal structures (top), PXRD (bottom), and PL microscope photos (inserted in PXRD) of (a) $(Pr_3BzN)_2SbCl_5$ and (b) $(Pr_3BzN)_2Sb_2Cl_8$.

$A_2Sb_2Cl_8$. The same $A_2Sb_2Cl_8$ product was obtained from this reaction, indicating the formation of the desired structure was solvent driven instead of stoichiometry driven. Full experimental details can be found in the Supporting Information. Significant structural differences between the A_2SbCl_5 and $A_2Sb_2Cl_8$ series were revealed via single crystal X-ray diffraction (SC-XRD). The phase purities of all samples were confirmed via powder X-ray diffraction (PXRD, Figure 1, Figure S1 and S2).

The molecular structures of the A_2SbCl_5 and $A_2Sb_2Cl_8$ series all revealed 0D antimony chlorides (Figure 2). The antimony chlorides synthesized from DMF has 5-coordiantated square pyramidal $[SbCl_5]$ geometry for the metal center, whereas the ones synthesize from HCl has 4-coordiantated seesaw dimer $[Sb_2Cl_8]$ geometry. The newly reported structure $(Pr_3BzN)_2Sb_2Cl_8$ crystallized in space group $P\bar{1}$. All crystallographic results and structural refinement details can be found in Table S1–S3.

The axial position Sb–Cl bonds for all structures are in similar values of each other (2.36–2.41 Å). However, the Sb–Cl bonds in equatorial plane have significant differences when comparing the A_2SbCl_5 and $A_2Sb_2Cl_8$ series. For A_2SbCl_5 series, all equatorial Sb–Cl bonds are in the range of 2.5–2.7 Å (Table 1).

In contrast to the A_2SbCl_5, one of the Sb–Cl distances in $A_2Sb_2Cl_8$ is elongated to greater than 2.90 Å, which resulted in trans effect that shortens the opposite Sb–Cl bond to $\leq$2.5 Å (Table 1). For $(Me_3BzN)_2SbCl_5$ and $(Et_3BzN)_2SbCl_5$, the longest Sb···Cl distances are 2.94 and 2.90 Å, respectively. These distances are much longer than average Sb–Cl bonds, but still considered as a bond based on some literatures.[40,44] However, for $(Pr_3BzN)_2Sb_2Cl_8$, $(Et_4N)_2Sb_2Cl_8$, and $(Pr_4N)_2Sb_2Cl_8$, the elongated Sb···Cl distances are

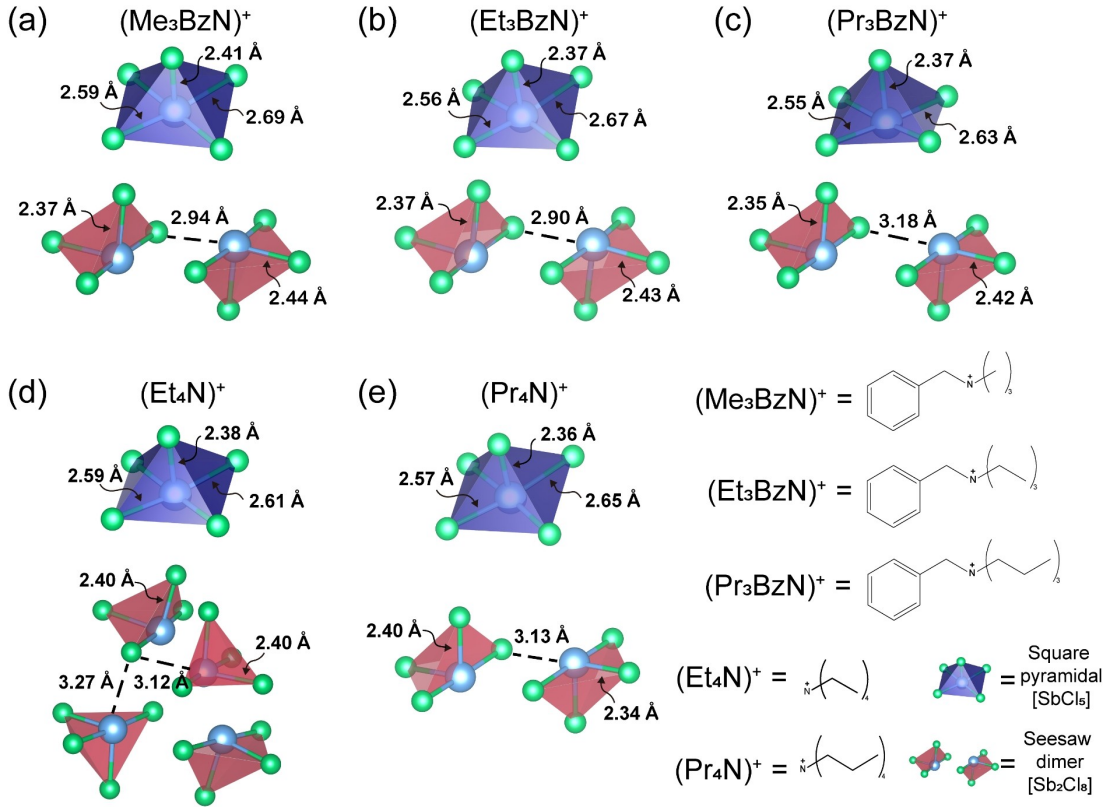

Figure 2. Coordination environments for all ten antimony chlorides discussed in this work. Antimony chlorides of A_2SbCl_5 are represented in dark blue; antimony chlorides of $A_2Sb_2Cl_8$ are represented in red.

greater than 3 Å, which are much deviant from the shortest bonds ≈2.3 Å. Therefore, they should no longer be considered as a bond.

Besides the intramolecular differences in Sb···Cl distances, large intermolecular differences in the Sb···Sb distances were also observed between the two series (Table 1). For the A_2SbCl_5, all Sb···Sb distances are greater than 8 Å (Figure 3). The trend of $(Me_3BzN)_2SbCl_5$, $(Et_3BzN)_2SbCl_5$, $(Pr_3BzN)_2SbCl_5$ follows that bulkier organic cation with longer alkyl chain showing larger separation between antimony chlorides. Although the shortest Sb···Sb distance of $(Et_3BzN)_2SbCl_5$ (8.80 Å) is shorter than that of $(Me_3BzN)_2SbCl_5$, the average Sb···Sb distance of them still follows expected trend. The two A_2SbCl_5 without benzyl group in organic cations follows the same trend with $(Pr_4N)_2SbCl_5$ having larger separation than $(Et_4N)_2SbCl_5$.

On the contrary, the shortest Sb···Sb distances for the $A_2Sb_2Cl_8$ series are in the range of 4.18–4.52 Å, suggesting a completely different coordination environment of the antimony chlorides. Same trend of bulkier organic cation producing larger separation of the antimony chlorides is observed for $(Me_3BzN)_2SbCl_5$, $(Et_3BzN)_2SbCl_5$, and $(Pr_3BzN)_2SbCl_5$, with $(Pr_3BzN)_2Sb_2Cl_8$ having the largest Sb···Sb distances (4.52 Å). However, the two A_2SbCl_5 without benzyl group, $(Pr_4N)_2SbCl_5$ and $(Et_4N)_2SbCl_5$ do not follow the same trend. This could be due to the organic cations being more flexible than the ones with benzyl group, leading to different packing in the crystal lattice. Regardless of the packing for these structures, all of the shortest Sb···Sb distances for the $A_2Sb_2Cl_8$ series are much shorter compared to the A_2SbCl_5 series.

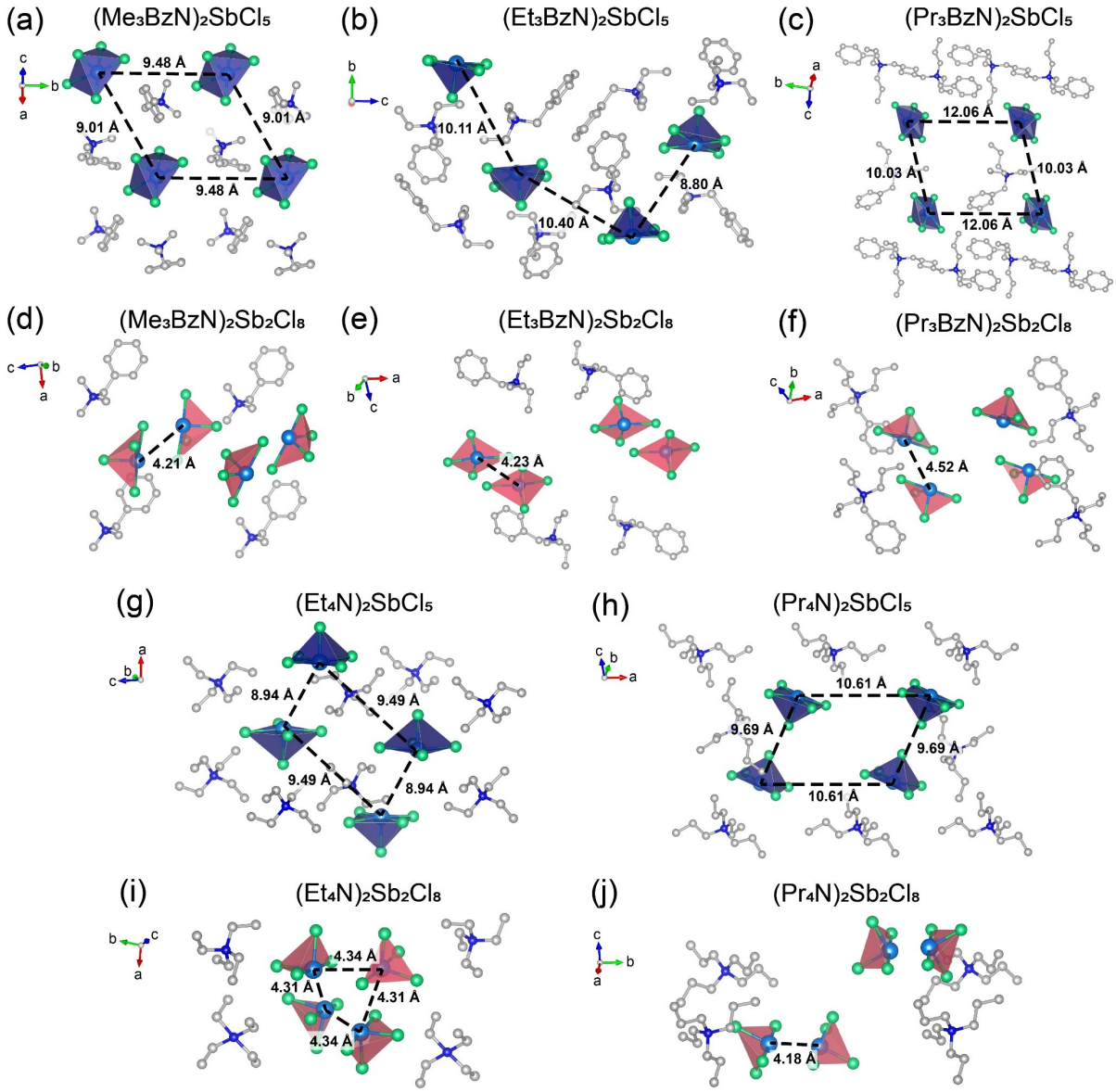

Figure 3. Structures of all antimony chlorides discussed in this work. Antimony chlorides of A_2SbCl_5 are represented in dark blue; antimony chlorides of $A_2Sb_2Cl_8$ are represented in red.

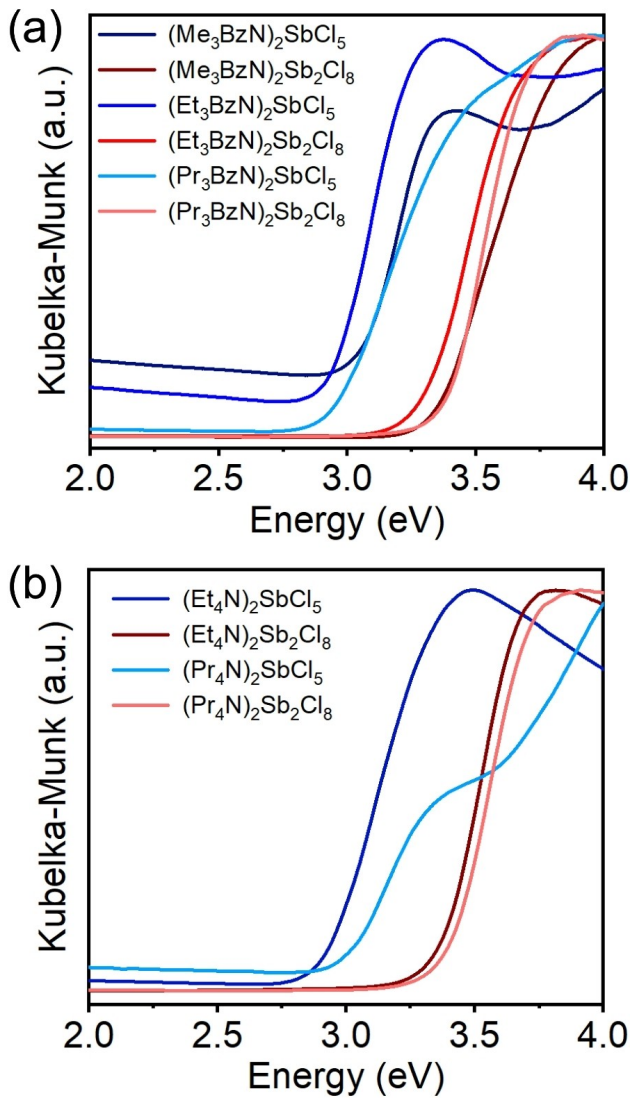

Figure 4. Normalized UV/Vis spectra of all antimony chlorides discussed in this work. The square pyramidal [$SbCl_5$] are represented in blue; the seesaw dimer [Sb_2Cl_8] are represented in red.

The band gaps of both A_2SbCl_5 and $A_2Sb_2Cl_8$ series were determined via UV/Vis spectroscopy. The determined values of the two series revealed characteristic differences in their optical properties. The band gaps of square pyramidal [$SbCl_5$] are in the range of 2.9–3.0 eV (Figure 4, Table 2). The band gaps of seesaw dimer [Sb_2Cl_8] are in a higher energy range of 3.3–3.4 eV. When comparing each pair of A_2SbCl_5 and $A_2Sb_2Cl_8$, there is always greater than 0.3 eV differences with same trend of $A_2Sb_2Cl_8$ having higher energy band gap. The antimony chlorides in A_2SbCl_5 and $A_2Sb_2Cl_8$ have different structures with one being square pyramidal and the other as seesaw dimmer. This indicates the two series may have different orbital overlaps between Sb and Cl that lead to significant change in energy of HOMO and LUMO. The band gaps are similar within each series (<0.1 eV difference), suggesting the organic cations has negligible effect on the energy.

Further investigation of optical properties was conducted through PL measurements of the antimony chlorides. All PL spectra of the A_2SbCl_5 series showed broad emission bands in the range of 550–700 nm (Figure 5a, b, and Table 2), consistent with the STE emission features observed for similar 0D antimony chlorides reported in the literature (Table 3). The shifts of these STE emission in the A_2SbCl_5 series are expected as each compound has different organic cations that leads to minor differences in their structural parameters. The lifetimes of these emission bands were found in close proximity to each other at the scale of ≈ 4 µs (Figure 5d, Table 2). It has been known that the strong broadband STE emission of Sb^{3+} originates from the transition of triplet $^3P_{n=2,1,0}$ to ground state $^1S_0$.[29,45,46] However, the structural differences between the A_2SbCl_5 and $A_2Sb_2Cl_8$ series may result in different orientation of the $5s^2$ lone pair of Sb^{3+} (as shown in Scheme 1). This difference may further lead to modulation of the PL properties, which is exactly what we observe in the characterization of the two series.

There are no PL spectra reported in the literature for structures similar to the $A_2Sb_2Cl_8$ series, likely due to their poor emission properties. Visually, no PL was observed for the $A_2Sb_2Cl_8$ series under 365 nm UV irradiation. In

Table 2: Comparison between PL emission, PLQY, and band gaps of the A_2SbCl_5 and $A_2Sb_2Cl_8$ series.

Organic Cation	type	$(Me_3BzN)^+$	$(Et_3BzN)^+$	$(Pr_3BzN)^+$	$(Et_4N)^+$ [a]	$(Pr_4N)^+$ [b]
Optical bandgap (eV)	[$SbCl_5$]	3.01	2.93	2.95	2.93	2.97
	[Sb_2Cl_8]	3.34	3.31	3.39	3.37	3.40
PL lifetime (µs)	[$SbCl_5$]	4.16	3.83	4.74	4.98	4.28
	[Sb_2Cl_8]	*N/A*	*N/A*	*N/A*	*N/A*	*N/A*
PLQY (%)	[$SbCl_5$]	95.3	97.0	96.3	97.3	94.9
	[Sb_2Cl_8]	~0	~0	~0	~0	~0
PL (em@ex, nm)	[$SbCl_5$]	620@351	589@367	640@372	627@373	610@357
	[Sb_2Cl_8]	*N/A*	*N/A*	*N/A*	*N/A*	*N/A*

[a] The measurements were performed using samples synthesized based on ref. [25, 26, 41, 42]. [b] The measurements were performed using samples synthesized based on ref. [42] and [43].

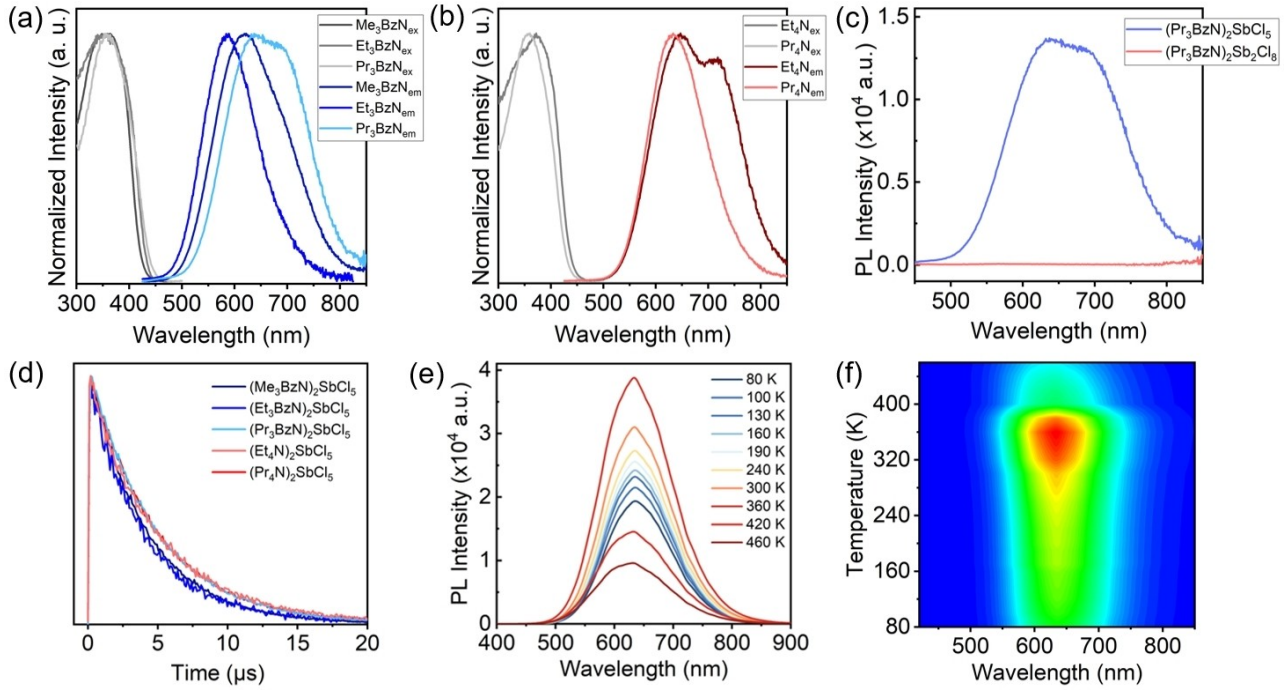

Figure 5. a) Normalized PL spectra for $(Me_3BzN)_2SbCl_5$, $(Et_3BzN)_2SbCl_5$, $(Pr_3BzN)_2SbCl_5$. b) Normalized PL spectra for $(Et_4N)_2SbCl_5$ and $(Pr_4N)_2SbCl_5$. c) Overlayed PL spectra for $(Pr_3BzN)_2SbCl_5$ and $(Pr_3BzN)_2Sb_2Cl_8$. d) Normalized plot for PL decay of the A_2SbCl_5 series. e) Temperature-dependent PL spectra of $(Pr_3BzN)_2SbCl_5$ excited with 405 nm laser. f) Intensity plot for temperature dependent PL measurements, PL intensity decreases from red to blue region.

Table 3: Summary of the PL properties of hybrid antimony chlorides listed in Figure 6.

Compound	Emission (nm)	PLQY (%)	PL Lifetime (μs)	Sb-Sb distance (Å)	Compound	Emission (nm)	PLQY (%)	PL Lifetime (μs)	Sb-Sb distance (Å)
$(Me_3BzN)_2SbCl_5$	620	95.3	4.16	9.00	$(Bmim)_2SbCl_5$	583	86.3	4.26	9.02
$(Et_3BzN)_2SbCl_5$	589	97.0	3.83	8.80	$(C_9NH_{20})_2SbCl_5$	590	98	4.2	8.76
$(Pr_3BzN)_2SbCl_5$	640	96.3	4.74	10.03	$(Ph_4P)_2SbCl_5$	650	87	4.57	9.17
$(Et_4N)_2SbCl_5$	627	97.3	4.98	9.46	$(PPN)_2SbCl_5$	635	98.1	4.1	12.19
$(Pr_4N)_2SbCl_5$	610	94.9	4.28	9.69	$(DTA)_2SbCl_5{\cdot}DTAC$	620	90	5.1	9.09
$(Me_3BzN)_2Sb_2Cl_8$	N/A	~0	N/A	4.21	$(HL)_3SbCl_5{\cdot}Cl$	566	99	4.33	8.79
$(Et_3BzN)_2Sb_2Cl_8$	N/A	~0	N/A	4.23	$(TMA)_2SbCl_5{\cdot}DMF$	630	67.2	6.62	8.61
$(Pr_3BzN)_2Sb_2Cl_8$	N/A	~0	N/A	4.52	$(C_6N_2H_{16})_2SbCl_5$	613	25.3	1.06	3.99
$(Et_4N)_2Sb_2Cl_8$	N/A	~0	N/A	4.31	$(C_6N_2H_{16})_2SbCl_5{\cdot}H_2O$	620	39.6	1.22	4.34
$(Pr_4N)_2Sb_2Cl_8$	N/A	~0	N/A	4.18					

*Data points of the compounds on the left section are collected in this work, some of which have been reported previously.[25,26,38-43] Data points of the compounds on the right section are reported values in literatures.[26–28,36,37,55–58]

addition, multiple experiments were performed, including PL (Xe source and 365 nm laser source) and PLQY measurements to confirm that the $A_2Sb_2Cl_8$ series do not exhibit PL (Table 2) at room temperature and even at low temperature down to 80 K. This observation confirms a large difference between the A_2SbCl_5 and $A_2Sb_2Cl_8$ series in their emission properties. For example, the overlay plot (Figure 5c) of $(Pr_3BzN)_2SbCl_5$ and $(Pr_3BzN)_2Sb_2Cl_8$ shows that the square pyramidal $[SbCl_5]$ has emission at 650 nm, whereas the seesaw dimer $[Sb_2Cl_8]$ exhibits no PL emission.

Furthermore, temperature dependent PL measurements (80–460 K) were performed to probe the PL properties of $(Pr_3BzN)_2SbCl_5$ (Figure 5e, f), $(Pr_3BzN)_2Sb_2Cl_8$, and $(Me_3BzN)_2SbCl_5$ (Figure S3). No PL features were observed for $(Pr_3BzN)_2Sb_2Cl_8$ at our probed temperature range (80–460 K). Unexpectedly, the PL intensity was found to be the strongest at 360 K for $(Pr_3BzN)_2SbCl_5$ and 340 K for $(Me_3BzN)_2SbCl_5$. This is unusual as most metal chlorides have stronger PL intensities at lower temperature, i.e. thermal quenching.[47–49] Similar anti-thermal quenching phenomena have also been observed in few other 0D luminous antimony chlorides,[24] and tin chlorides.[50] It further confirms the STE emission mechanism of $(Pr_3BzN)_2SbCl_5$ and $(Me_3BzN)_2SbCl_5$. There is an energy barrier from the excited non-emissive state to the bright STE emission state, which can be conquered by thermal activation. Therefore, as temperature increases from 80 to 360 K, more excitons are activated to the emissive STE state, resulting in enhanced PL intensity. The PL spectrum also becomes broader in higher temperature, which indicates the thermal enhanced electron-phonon coupling effect. Meanwhile, higher temperatures also lead to a larger thermal quenching via non-radiative pathways which reduces the PL intensity. The interplay between thermal activation and quenching results in the PL intensity approaching the maximum at 360 K.

The corresponding temperature dependent PL lifetime measurements (80–320 K) were performed for $(Me_3BzN)_2SbCl_5$ and $(Pr_3BzN)_2SbCl_5$ (Figure S4). The exponential decay curves show consistent mechanism throughout the measured temperature range, whereas the lifetime prolongs with decreasing temperature. The monitored PL lifetimes of $(Me_3BzN)_2SbCl_5$ and $(Pr_3BzN)_2SbCl_5$ increased through the cooling process, indicating enhancement of the broadband STE emission as the temperature decrease.

The differences in Sb···Sb, Sb–Cl distances, and PLQY lead us to further dive into literature to seek deeper understanding on how structures may affect the electronic properties of the antimony chlorides. We extracted additional information from reported structures and combined with our data to obtain a correlation plot (Figure 6, Table 3). Majority of the antimony chlorides with A_2SbCl_5 form has large Sb···Sb distances (>8 Å) and high PLQY (blue circles in Figure 6). There is no information reported on the PLQY of $A_2Sb_2Cl_8$ series, so all PLQY of the $A_2Sb_2Cl_8$ series are our experimental results (red circles in Figure 6). The correlation plot clearly demonstrates the antimony chlorides with larger Sb···Sb distances have stronger PLQY, and vice versa. This trend is also observed in similar fashion as the correlation of Mn···Mn distances and PLQY, which exhibit similar effect as concentration quenching in a doped system.[51] The correlation is attributed to easier energy transfer caused by dipole–dipole interactions and symmetry-directed spin-exchange interactions.[35,52] It stands well with the same structural type because the square pyramidal $[SbCl_5]$ usually leads to far separation that produce high PLQY. On the other hand, extended structures such as $A_3Sb_2X_9$ type 2D (111)-oriented perovskites, are usually non-emissive.[53,54]

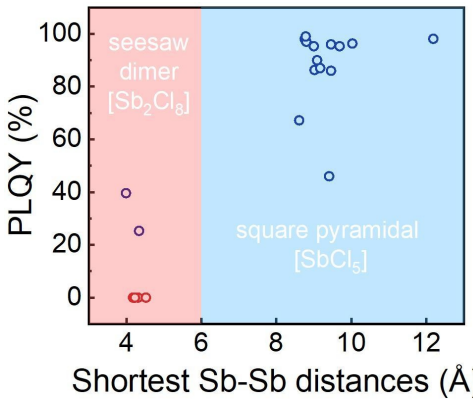

Figure 6. Correlation between Sb···Sb distances and PLQY based on our experimental results and literature reports. The blue circles represent A_2SbCl_5, and the red circles represent $A_2Sb_2Cl_8$. Further discussion revolves around the two blue circle data points has been provided in the main text.

However, some of the outliers in the plot caught our attention. First, the $(MeEt_3N)_2SbCl_5$ has much lower PLQY (46 %) even though its shortest Sb···Sb distance falls into the range of >8 Å. We have re-synthesized the $(MeEt_3N)_2SbCl_5$ and found it to be relatively unstable under ambient conditions (Figure S6), possibly affecting the measured PLQY results. This outlier suggests that not only the optical properties, but also the stability of the antimony halides should be considered as a possible factor affecting its PL performance.

Furthermore, Lin et al.[55] showed two structures, $(C_6N_2H_{16})SbCl_5$ and $(C_6N_2H_{16})SbCl_5{\cdot}H_2O$, both having square pyramidal $[SbCl_5]$ geometry. The shortest Sb···Sb distances of $(C_6N_2H_{16})SbCl_5$ and $(C_6N_2H_{16})SbCl_5{\cdot}H_2O$ are 4.34 and 3.99 Å, respectively, which falls in the short end of the correlation plot (Figure 6). These antimony chlorides still have PLQY of 25.3 and 39.6 %, listed in Figure 6 as the two data points off the trend. The moderate PLQY could rise from contradiction of coordination environment being square pyramidal favors high PLQY while the short Sb···Sb distances favors low PLQY. The authors discussed that the addition of the H_2O molecule may separate the antimony chlorides further apart from each other, with Sb···Cl distances became longer and PLQY became higher. However, when looking into the detailed structural parameters of these two antimony chlorides, additional H_2O molecule shortened the Sb···Sb distance, yet the PLQY still became higher. These structural parameters suggest that when looking at structure-PL property relationships, a more cohesive consideration is needed instead of counting a single factor as full contribution. Other factors such as the morphology (nanocrystal vs. bulk), quality of the sample (powder vs. single-crystal) also make a difference in PLQY.

To gain better insight in the electronic structure of the two series, DFT calculations were performed on a pair of the antimony chlorides, $(Pr_3BzN)SbCl_4$ and $(Pr_3BzN)_2SbCl_5$ (Figure 7). The calculated electronic band gaps of $(Pr_3BzN)SbCl_4$ and $(Pr_3BzN)_2SbCl_5$ have been identified as

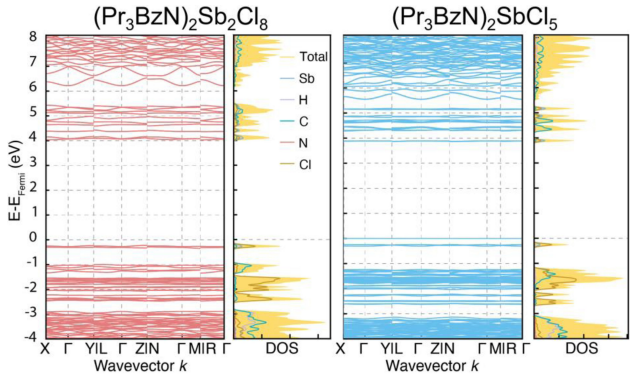

Figure 7. DFT (HSE06 with spin-orbit coupling) calculated band structure and projected density of states (pDOS) of $(Pr_3BzN)_2Sb_2Cl_8$ (left) and $(Pr_3BzN)_2SbCl_5$ (right). The Fermi energy (E_{Fermi}) has been set as 0.

an indirect band gap of 4.25 eV (Z to R) and a direct band gap of 4.05 eV (N to N), respectively. The predicted band gaps are larger than the experimental value of 2.95 and 3.39 eV, due to overestimation from the HSE06 hybrid functional. However, the trend of the band gaps for antimony chlorides having square pyramidal [$SbCl_5$] lower than the seesaw dimer [Sb_2Cl_8] agrees with the experimental results. Both antimony chlorides contain relatively flat band dispersion, which implies poor charge carrier transport properties.

Conclusion

We have successfully optimized the synthetic condition to target the formation of specific coordination environment for the antimony chlorides, which leads to two series of antimony chlorides with square pyramidal and seesaw geometries, respectively. With this strategy, many non-emissive Sb^{III} halides reported previously may be able to transform into emissive materials. Incorporating large organic cations, all A_2SbCl_5 compounds with square pyramidal [$SbCl_5$] geometry are found to have near unity PLQY, whereas the $A_2Sb_2Cl_8$ compounds with seesaw dimer [Sb_2Cl_8] geometry have PLQY $\approx$ 0 % at room temperature. Moreover, the two series have signature optical band gap trends where the A_2SbCl_5 type always has narrower gap than the corresponding $A_2Sb_2Cl_8$ type. With a comprehensive database analysis, we have found that multiple factors such as coordination environments, Sb···Sb distances, Sb–Cl bond lengths, and stability of the material have impacts on the PL emission and PLQY. Therefore, the structure–property relationships of antimony chlorides should be considered with multiple factors instead of dictated by a single contributor. Our synthetic and structural guidelines provide a useful handle to directly achieve high PLQY materials and further mechanistic insights towards next generation optoelectronic materials design.

Acknowledgements

This work was supported by the National Natural Science Foundation of China (NSFC) under Grant No. 22275077, the Stable Support Plan Program of Shenzhen Natural Science Fund (Program Contract No. 20220814233319001), and the Startup Fund of SUSTech. The authors are grateful for the assistance of SUSTech Core Research Facilities.

Conflict of Interest

The authors declare no conflict of interest.

Data Availability Statement

The data that support the findings of this study are available from the corresponding author upon reasonable request.

Keywords: Antimony Halide · Hybrid Materials · Luminescent Materials · Photoluminescence Quantum Yield · Structure–Property Relationship

[1] N. J. Jeon, J. H. Noh, W. S. Yang, Y. C. Kim, S. Ryu, J. Seo, S. I. Seok, *Nature* **2015**, *517*, 476–480.
[2] M. Saliba, T. Matsuii, K. Domansk, J.-Y. Seo, A. Ummadis-tingu, S. M. Zakeeruddin, J.-P. Correa-Baena, W. R. Tress, A. Abate, A. Hagfeldt, M. Grätzel, *Science* **2016**, *354*, 206–209.
[3] S. D. Stranks, H. J. Snaith, *Nat. Nanotechnol.* **2015**, *10*, 391–402.
[4] H. Cho, S.-H. Jeong, M.-H. Park, Y.-H. Kim, C. Wolf, C.-L. Lee, H. H. Kheo, A. Sadhanala, N. Myoung, S. Yoo, S. H. Im, R. H. Friend, T.-W. Lee, *Science* **2015**, *350*, 1222–1225.
[5] X. K. Liu, W. Xu, S. Bai, Y. Jin, J. Wang, R. H. Friend, F. Gao, *Nat. Mater.* **2021**, *20*, 10–21.
[6] L. Mao, C. C. Stoumpos, M. G. Kanatzidis, *J. Am. Chem. Soc.* **2019**, *141*, 1171–1190.
[7] L. Mao, J. Chen, P. Vishnoi, A. K. Cheetham, *Acc. Mater. Res.* **2022**, *3*, 439–448.
[8] M. D. Smith, B. A. Connor, H. I. Karunadasa, *Chem. Rev.* **2019**, *119*, 3104–3139.
[9] C. C. Stoumpos, M. G. Kanatzidis, *Adv. Mater.* **2016**, *28*, 5778–5793.
[10] A. Zanetta, Z. Andaji-Garmaroudi, V. Pirota, G. Pica, F. U. Kosasih, L. Gouda, K. Frohna, C. Ducati, F. Doria, S. D. Stranks, G. Grancini, *Adv. Mater.* **2022**, *34*, e2105942.
[11] S. Adjokatse, H.-H. Fang, M. A. Loi, *Mater. Today* **2017**, *20*, 413–424.
[12] Q. He, C. Zhou, L. Xu, S. Lee, X. Lin, J. Neu, M. Worku, M. Chaaban, B. Ma, *ACS Mater. Lett.* **2020**, *2*, 633–638.
[13] V. Morad, S. Yakunin, M. V. Kovalenko, *ACS Mater. Lett.* **2020**, *2*, 845–852.
[14] Y. Liu, Y. P. Gong, S. Geng, M. L. Feng, D. Manidaki, Z. Deng, C. C. Stoumpos, P. Canepa, Z. Xiao, W. X. Zhang, L. Mao, *Angew. Chem. Int. Ed.* **2022**, *61*, e202208875; *Angew. Chem.* **2022**, *134*, e202208875.
[15] G. Laurita, R. Seshadri, *Acc. Chem. Res.* **2022**, *55*, 1004–1014.
[16] K. M. McCall, V. Morad, B. M. Benin, M. V. Kovalenko, *ACS Mater. Lett.* **2020**, *2*, 1218–1232.
[17] Y. Jing, Y. Liu, X. Jiang, M. S. Molokeev, Z. Lin, Z. Xia, *Chem. Mater.* **2020**, *32*, 5327–5334.

[18] G. Zhang, P. Dang, H. Xiao, H. Lian, S. Liang, L. Yang, Z. Cheng, G. Li, J. Lin, *Adv. Opt. Mater.* **2021**, *9*, 2001766.
[19] M. B. Gray, S. Hariyani, T. A. Strom, J. D. Majher, J. Brgoch, P. M. Woodward, *J. Mater. Chem. C* **2020**, *8*, 6797–6803.
[20] T. V. Sedakova, A. G. Mirochnik, V. E. Karasev, *Opt. Spectrosc.* **2008**, *105*, 517–523.
[21] D.-Y. Li, Y. Cheng, Y.-H. Hou, J.-H. Song, C.-J. Sun, C.-Y. Yue, Z.-H. Jing, X.-W. Lei, *J. Chem. C* **2022**, *10*, 3746–3755.
[22] J.-Q. Zhao, H.-S. Shi, L.-R. Zeng, H. Ge, Y.-H. Hou, X.-M. Wu, C.-Y. Yue, X.-W. Lei, *Chem. Eng. J.* **2022**, *431*, 134336.
[23] D.-Y. Li, J.-H. Song, Z.-Y. Xu, Y.-J. Gao, X. Yin, Y.-H. Hou, L.-J. Feng, C.-Y. Yue, H. Fei, X.-W. Lei, *Chem. Mater.* **2022**, *34*, 6985–6995.
[24] J. L. Li, Y. F. Sang, L. J. Xu, H. Y. Lu, J. Y. Wang, Z. N. Chen, *Angew. Chem. Int. Ed.* **2022**, *61*, e202113450; *Angew. Chem.* **2022**, *134*, e202113450.
[25] Z. Li, Y. Li, P. Liang, T. Zhou, L. Wang, R.-J. Xie, *Chem. Mater.* **2019**, *31*, 9363–9371.
[26] Z. Wang, D. Xie, F. Zhang, J. Yu, X. Chen, C. P. Wong, *Sci. Adv.* **2020**, *6*, eabc2181.
[27] Q. He, C. Zhou, L. Xu, S. Lee, X. Lin, J. Neu, M. Worku, M. Chaaban, B. Ma, *ACS Mater. Lett.* **2020**, *2*, 633–638.
[28] F. Liu, T. Zhang, D. Mondal, S. Teng, Y. Zhang, K. Huang, D. Wang, W. Yang, P. Mahadevan, Y. S. Zhao, R. Xie, N. Pradhan, *Angew. Chem. Int. Ed.* **2021**, *60*, 13548–13553; *Angew. Chem.* **2021**, *133*, 13660–13665.
[29] M. Li, J. Lin, N. Wang, K. Liu, L. Fan, Z. Guo, W. Yuan, J. Zhao, Q. Liu, *Inorg. Chem.* **2022**, *61*, 15016–15022.
[30] Y. C. Peng, S. H. Zhou, J. C. Jin, Q. Gu, T. H. Zhuang, L. K. Gong, Z. P. Wang, K. Z. Du, X. Y. Huang, *Dalton Trans.* **2022**, *51*, 4919–4926.
[31] C. Zhou, L. J. Xu, S. Lee, H. Lin, B. Ma, *Adv. Opt. Mater.* **2021**, *9*, 2001766.
[32] S. Li, J. Luo, J. Liu, J. Tang, *J. Phys. Chem. Lett.* **2019**, *10*, 1999–2007.
[33] H. Lin, C. Zhou, Y. Tian, T. Siegrist, B. Ma, *ACS Energy Lett.* **2018**, *3*, 54–62.
[34] G. Zhou, B. Su, J. Huang, Q. Zhang, Z. Xia, *Mater. Sci. Eng. C* **2020**, *141*, 100548.
[35] L. Mao, P. Guo, S. Wang, A. K. Cheetham, R. Seshadri, *J. Am. Chem. Soc.* **2020**, *142*, 13582–13589.
[36] C. Zhou, M. Worku, J. Neu, H. Lin, Y. Tian, S. Lee, Y. Zhou, D. Han, S. Chen, A. Hao, P. I. Djurovich, T. Siegrist, M.-H. Du, B. Ma, *Chem. Mater.* **2018**, *30*, 2374–2378.
[37] F. Lin, H. Tong, H. Lin, W. Liu, *Chem. Commun.* **2022**, *58*, 125896–12599.
[38] M. S. Molokeev, B. Su, A. S. Aleksandrovsky, N. N. Golovnev, M. E. Plyaskin, Z. Xia, *Chem. Mater.* **2022**, *34*, 537–546.
[39] H. Peng, Y. Tian, Z. Yu, X. Wang, B. Ke, Y. Zhao, T. Dong, J. Wang, B. Zou, *Sci. China Mater.* **2022**, *65*, 1594–1600.
[40] B. Su, S. Geng, Z. Xiao, Z. Xia, *Angew. Chem. Int. Ed.* **2022**, *61*, e202208881; *Angew. Chem.* **2022**, *134*, e202208881.
[41] J. Zaleski, *Ferroelectrics* **1997**, *192*, 71–79.
[42] U. Ensinger, W. Schwarz, A. Schmidt, *Z. Naturforsch. B* **1982**, *37*, 1584–1589.
[43] H. Peng, Y. Tian, X. Wang, T. Huang, Y. Xiao, T. Dong, J. Hu, J. Wang, B. Zou, *J. Mater. Chem. C* **2021**, *9*, 12184–12190.
[44] B. Jaschinski, R. Blachnik, H. Reuter, *Z. Anorg. Allg. Chem.* **1999**, *625*, 667–672.
[45] L. Zhou, J. F. Liao, D. B. Kuang, *Adv. Opt. Mater.* **2021**, *9*, 2100544.
[46] N. Shen, Z. Wang, J. Jin, L. Gong, Z. Zhang, X. Huang, *CrystEngComm* **2020**, *22*, 3395–3405.
[47] G. Blasse, B. C. Grabmaier, *Luminescent Materials*, Springer, Berlin, **1994**.
[48] J. Chen, Y. Zhao, Z. Mao, D. Wang, L. Bie, *J. Lumin.* **2017**, *186*, 72–76.
[49] P. Yu, W. Liu, T. Shao, P. Gao, B. Jiang, C. Liu, Z. Ma, *Opt. Mater.* **2021**, *119*, 111379.
[50] B.-B. Zhang, J.-K. Chen, J.-P. Ma, X.-F. Jia, Q. Zhao, S.-Q. Guo, Y.-M. Chen, Q. Liu, Y. Kuroiwa, C. Moriyoshi, J. Zhang, H.-T. Sun, *J. Phys. Chem. Lett.* **2020**, *11*, 2902–2909.
[51] H.-Y. Chen, S. Maiti, D. H. Son, *ACS Nano* **2012**, *6*, 583–591.
[52] Y. Liu, J. Zhang, B. Han, X. Wang, Z. Wang, C. Xue, G. Bian, D. Hu, R. Zhou, D. S. Li, Z. Wang, Z. Ouyang, M. Li, T. Wu, *J. Am. Chem. Soc.* **2020**, *142*, 6649–6660.
[53] B. Saparov, F. Hong, J.-P. Sun, H.-S. Duan, W. Meng, S. Cameron, I. G. Hill, Y. Yan, D. B. Mitzi, *Chem. Mater.* **2015**, *27*, 5622–5632.
[54] K. M. McCall, C. C. Stoumpos, S. S. Kostina, M. G. Kanatzidis, B. W. Wessels, *Chem. Mater.* **2017**, *29*, 4129–4145.
[55] G. Song, M. Li, S. Zhang, N. Wang, P. Gong, Z. Xia, Z. Lin, *Adv. Funct. Mater.* **2020**, *30*, 2002468.
[56] Z. P. Wang, J. Y. Wang, J. R. Li, M. L. Feng, G. D. Zou, X. Y. Huang, *Chem. Commun.* **2015**, *51*, 3094–3097.
[57] C. Zhou, H. Lin, Y. Tian, Z. Yuan, R. Clark, B. Chen, L. J. van de Burgt, J. C. Wang, Y. Zhou, K. Hanson, Q. J. Meisner, J. Neu, T. Besara, T. Siegrist, E. Lambers, P. Djurovich, B. Ma, *Chem. Sci.* **2018**, *9*, 586–593.
[58] Q. Wei, T. Chang, R. Zeng, S. Cao, J. Zhao, X. Han, L. Wang, B. Zou, *J. Phys. Chem. Lett.* **2021**, *12*, 7091–7099.
[59] Deposition Numbers 2218970, 2218971, 2218972, 2218973, 2218974, 2218975 contain the supplementary crystallographic data for this paper. These data are provided free of charge by the joint Cambridge Crystallographic Data Centre and Fachinformationszentrum Karlsruhe Access Structures service.

Manuscript received: November 13, 2022
Accepted manuscript online: January 9, 2023
Version of record online: January 25, 2023